Network RTK Versus Single Base RTK - Understanding the Error Characteristics

Ulrich Vollath, Herbert Landau, Xiaoming Chen, Ken Doucet, Christian Pagels

Trimble Terrasat GmbH, Hoehenkirchen, Germany

BIOGRAPHY

Dr. Ulrich Vollath received a Ph.D. in Computer Science from the Munich University of Technology (TUM) in 1993. At Trimble Terrasat - where he is working on GPS algorithms since almost ten years - he is responsible for the Department of Algorithm Development. His professional interest is focused on high-precision real-time kinematic positioning and reference station network processing.

Dr. Herbert Landau is Managing Director of Trimble Terrasat. He has many years of experience in GPS and has been involved in a large variety of GPS and GLONASS developments for high precision positioning systems and applications.

Dr. Xiaoming Chen is a software engineer at Trimble Terrasat. He holds a PhD in Geodesy from Wuhan Technical University of Surveying and Mapping.

Ken Doucet obtained a Bachelor of Science degree in Surveying Engineering from the University of New Brunswick in 1986. Since that time he has been involved in the development of software for surveying applications of GPS as a research officer with the Geodetic Survey of Canada, a research assistant with the University of New Brunswick and, currently, as a staff software engineer with Trimble Navigation based in Westminster Colorado.

Christian Pagels has a degree in Physics from the University of Erlangen (1993). He is Senior Development Engineer at Trimble Terrasat and working on the design of reference station systems.

ABSTRACT

The use of reference station networks has become the ubiquitous solution for high precision satellite positioning applications. The main systematic errors affecting the RTK rover performance are multipath, atmospheric and ephemeris errors. Whereas single base RTK is limited with respect to the distance between reference and rover the network RTK approach offers the possibility to increase the coverage area. It ideally leads to a situation in which the positioning error is independent of the rover position in the area of the network.

One technique proven in production systems for network RTK is the Virtual Reference Station paradigm, simulating a local reference station for the user. Ideally, this provides a data quality equivalent to a very close reference station.

This paper gives a quantitative assessment of the data characteristics leading to the known rover performance improvements using data from different RTK/VRS networks from Asia, Europe, Australia and the U.S.A.

One major effect from the application of VRS can be seen as a significant reduction of the temporal correlation of the ionospheric residual errors. Autocorrelation functions respective the autocorrelation time constants show this clearly. Improvements for multipath, tropospheric delay and ephemeris errors are achieved by VRS techniques, too.

Detailed analyses explain the reduction of initialization times, improvement in position accuracy and increase in reliability seen in network RTK systems. This is not only due to the mitigation of systematic errors. It is demonstrated that network RTK does not only reduce the errors but also changes the error characteristics which lead to an additional performance increase in RTK positioning.

The important conclusion of the presented results is that once these changes in the error characteristics are fully understood and accounted for, more improvements in the performance of Network RTK applications can be expected.

VIRTUAL REFERENCE STATIONS PRINCIPLE

The Virtual Reference Station (VRS) concept is in commercial and research use since several years. Instead of presenting it again here, we refer to existing publications on that topic ([4], [5], [6]).

To summarize, the VRS approach generates reference station data for every user as if coming from a local near reference station. For that purpose, a network of reference stations permanently tracks the errors in centimeter-level precision using ambiguity resolution techniques. To predict the errors for the user position, error models and

interpolation algorithms are used. Figure 1 shows a typical field setup for geodetic applications.
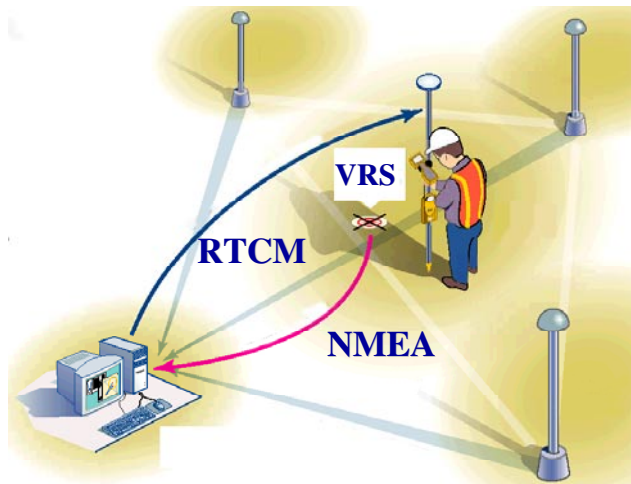

Figure 1: VRS field set-up procedure.

The receiver is started in the field. A coarse estimate of the receiver position is sent to the VRS network-computing center via e.g. cell phone. The center generates virtual reference station data for that position and transmits it in a standard format like RTCM enabling centimeter-level RTK operation for the user.

TEST GOALS

The significant effect of the VRS technique on productivity, reliability and precision of RTK positioning solutions has been observed many times ([8], [10]). One standard explanation for this used to be a "roughly two times reduction of ionosphere" and improvements in troposphere and orbit errors.

The aim of the investigations presented in this paper was to quantify the improvements of the measurement errors using a broad range of data from different parts of the world and varying seasons of the year.

Also, being aware that there are different kinds of error, a more sophisticated separation of the error characteristics was desired.

The approach taken in this project was to distinguish the errors based on their statistical properties:

- Time correlated errors

- Uncorrelated (white noise type) errors

- Biases

Still, ionospheric errors and geometric errors should be handled separately to get individual answers for these cases as modeling and interpolation mostly is done independently on both.

OBSERVABLE SELECTION

For every data set, the ambiguities were solved in post-processing. Then, the double-difference residuals were created using the precise position of the respective receiver antenna for the following phase combinations:

Ionospheric carrier phase combination, a.k.a. geometry-free combination:

$$\phi_{iono} = \left(\lambda_{L1} \cdot \phi_{L1} - \lambda_{L2} \cdot \phi_{L2} \right) \cdot \frac{\lambda_{L1}^2}{\lambda_{L2}^2 - \lambda_{L1}^2}$$

Geometric carrier phase combination ([2]):

$$\phi_{geo} = a \cdot \lambda_{L1} \cdot \phi_{L1} + (1-a) \cdot \lambda_{L2} \cdot \phi_{L2}$$

The geometric ranges between satellites and receivers and an a priori tropospheric model (modified Hopfield, [12]) were removed from the geometric residuals in the common way.

STATISTICAL CHARACTERIZATION

As mentioned before, the main goal was separation of the correlated and uncorrelated errors in the measurements.

A first assumption taken here is that the time correlation can be defined by an exponential function. Tests have shown that this at least is a quite realistic assumption for a broad range of errors seen in GPS observables, as are ionospheric and tropospheric residuals and multipath.

Given the presence of uncorrelated (white noise) errors together with exponentially time correlated errors, the variance/covariance matrix of one time series for the double differences to one satellite is given by:

$$C = \begin{pmatrix} \sigma_c^2 + \sigma_u^2 & \cdots & \sigma_c^2 \cdot e^{-\frac{\Delta t}{t_c}} & \cdots \\ \vdots & \ddots & \vdots & \cdots \\ \sigma_c^2 \cdot e^{-\frac{\Delta t}{t_c}} & \cdots & \sigma_c^2 + \sigma_u^2 & \cdots \\ \vdots & \vdots & \vdots & \ddots \end{pmatrix}$$

Conversion to the correlation matrix yields:

$$R = \begin{pmatrix} 1 & \cdots & \dfrac{\sigma_c^2}{\sigma_c^2 + \sigma_u^2} \cdot e^{-\frac{\Delta t}{t_c}} & \cdots \\ \vdots & \ddots & \vdots & \cdots \\ \dfrac{\sigma_c^2}{\sigma_c^2 + \sigma_u^2} \cdot e^{-\frac{\Delta t}{t_c}} & \cdots & 1 & \cdots \\ \vdots & \vdots & \vdots & \ddots \end{pmatrix}$$

In Figure 2 the resulting autocorrelation function

$$R(\Delta t) = \begin{cases} 1, \Delta t = 0 \\ \dfrac{\sigma_u^2}{\sigma_u^2 + \sigma_c^2} \cdot e^{-\frac{\Delta t}{t_c}}, \Delta t > 0 \end{cases}$$

is rendered. In these formulas, the following notations were used:

- σ_c: correlated noise standard deviation

- σ_u: correlated noise standard deviation
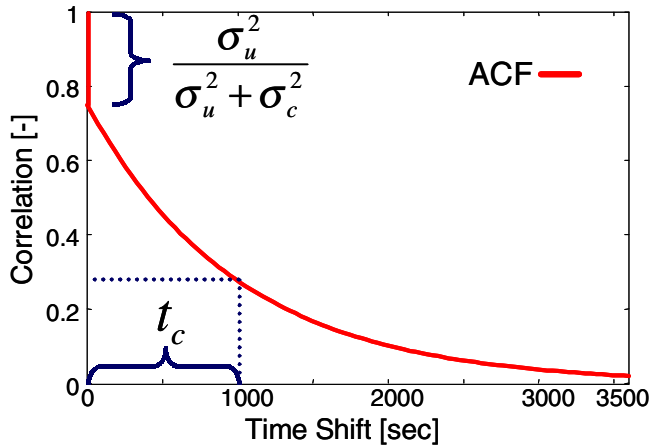
- t_c: time constant

Figure 2: Auto-Correlation function

There is a characteristic jump at a time delay of 0 that reflects the ratio between the uncorrelated and the total error. The decay of the function is defined by the correlation time, where $R(t_c) = \dfrac{\sigma_u^2}{\sigma_u^2 + \sigma_c^2} \cdot e^{-1}$ is the characteristic correlation pointing at the correlation time.

To compute the correlated error, time constant and uncorrelated error, this auto-correlation function was not directly used. The reason is that a curve fit to the ACF using 2 parameters is only weakly determined. Instead, a new statistical evaluation was implemented that directly derives the three parameters and gives reasonably answer for short time spans of data.

The importance of the separation of correlated and uncorrelated errors can be seen in Figure 2. If a simple exponential function $R(x) = e^{-\frac{\Delta t}{t_c}}$ is fitted to the ACF, the time constant will be estimated much too low.

In addition, the mean value for every residual time series was computed to reflect the systematic errors present in the data.

MOTIVATION

One question that could be posed here is why such an effort is necessary. In Figure 3 the difference between uncorrelated errors and time correlated errors can easily be seen for the formal evolution of the standard deviations of an estimate.
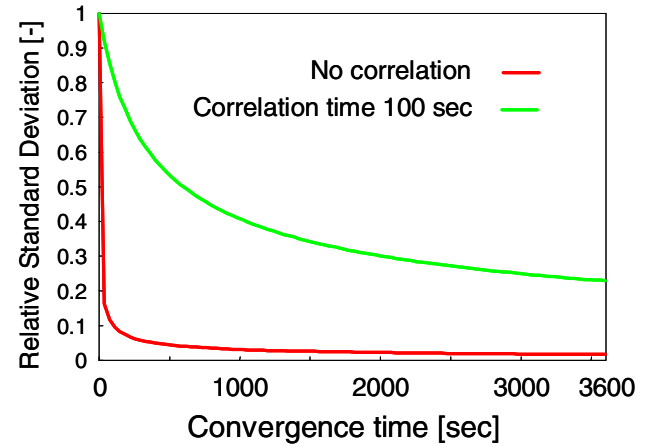
Figure 3: Convergence for white and correlated noise

All values are relative to the standard deviation of a single measurement. The uncorrelated time series errors reduce by far faster than for the correlated data. This has two consequences. The reduction of the time constant is crucial for fast convergence. This affects the time until ambiguities can be resolved (time-to-fix) as well as the time needed to acquire a given precision for a position computation (time-to-precision). Also, knowing the time constant, better predictions can be done for the accuracy reached after a given time of data accumulation. If the knowledge of the time correlation is limited, either the expected errors are too optimistic leading to a poor reliability or too pessimistic resulting in a poor availability and productivity.

TEST NETWORKS

Six networks (see Figure 4) operated with Trimble Terrasat GPSNet software were used for the analyses.
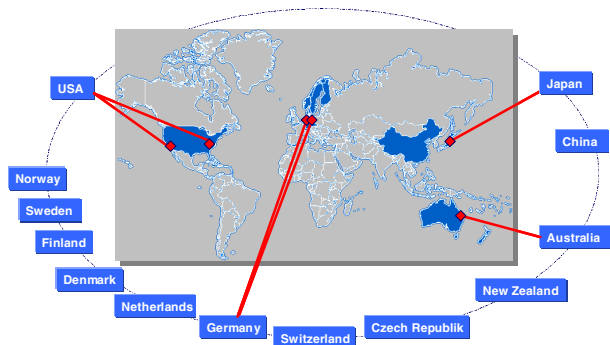
Figure 4: GPSNet VRS installations used for the tests

For every network, one reference receiver was taken out of the network processing and used as the user receiver (rover).

The following enumeration gives location, time of data collection and the distance of the rover station to the nearest reference station.

1. Queensland, Australia, February 2001, 31 km

2. Kanto, Japan, January 2002, 26 km

3. Thueringen, Germany, August 2002, 19 km

4. Bavaria, Germany, May 2002, 31 km

5. California, U.S.A., November 2001, 25 km

6. North Carolina, U.S.A., September 2002, 27 km

For every network, 24 hours of data were used to include day- and nighttime.

The data of the network stations excluding the rover station was processed using a post-processing version of the real-time VRS software GPSNet. Instead of the usual dial-in functionality to generate VRS RTCM data, the virtual reference station data was generated using the same algorithms but written into a post-processing file format.

Then a standard GPS post-processing software (Trimble Total Control) was used to determine the fixed ambiguities for the long baseline (rover to nearest reference station) and the VRS baseline.

Using these ambiguities and precise coordinates for the stations involved, the residuals were derived in the way described above. For every time series, i.e. every satellite double difference residuals series the auto-correlation analysis was performed.

ANALYSIS RESULTS

A typical example of the error reduction by VRS processing is shown in Figure 5 for the California network.
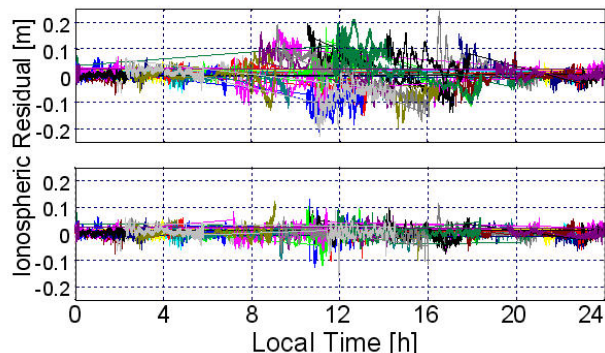

Figure 5: Ionospheric residuals without and with VRS

It can be clearly seen that the raw data (upper graph) includes a substantial increase of the ionospheric residuals during daytime. This is very much mitigated in the VRS data (lower graph). Though this is obvious, the detailed statistical analyses for all data lead to insights not available from a simple look at the data.

Table 1 (located at the end of this paper) presents a compilation of the analysis results. Correlation time t_{cor}, bias, correlated error standard deviation σ_{cor} and uncorrelated error standard deviation σ_{unc} are given for ionospheric and geometric residuals separately.

For every network, the raw data residuals, VRS residuals and the improvement factor between both are given. The last row gives the mean improvement factors over all networks.

The improvements are visualized in the following figures. They give bars for raw ionospheric residuals, VRS ionospheric residuals, raw geometric residuals and VRS geometric residuals respective.

The results are given for all networks separately and are labeled as follows:

- AUS: Australia network

- JP: Japan Network

- GER1: Thueringen, Germany

- GER2, Bavaria, Germany

- CA: California, U.S.A

- N.C.: North Carolina, U.S.A.

Figure 6 shows mainly the effects that were studied in the past, i.e. the improvements of the correlated errors as the main contribution.
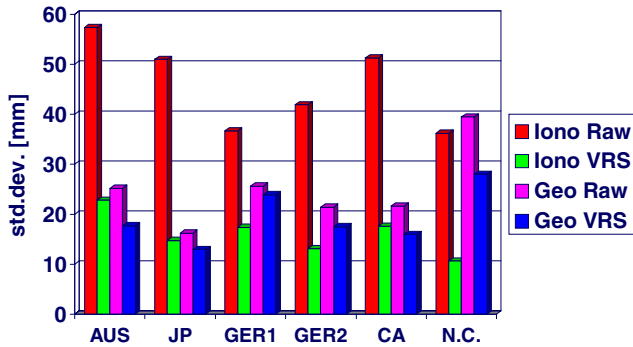
Figure 6: Correlated errors

Nevertheless, this information is not complete without a look at Figure 7 showing the time constants for the time-correlated errors. Especially for the ionosphere, a very high improvement can be seen. For the geometric error, the improvements are marginal. This should be subject to further studies.
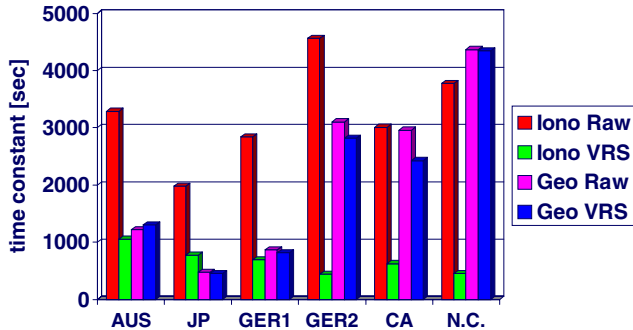

Figure 7: Time constants

The "noise part" of the errors is shown in Figure 8. The improvements are in the tens of percent range. One reason is that only the reference side can be influenced, while mitigation for the rover side is not possible. This applies to multipath which is not separately studies in this paper, too.

Still this is an advantage in kinematic applications where averaging in the position domain is not feasible.
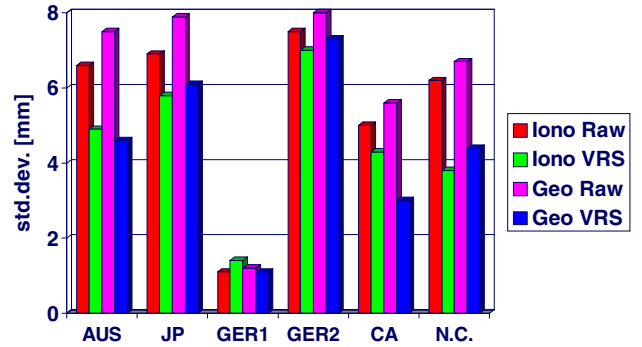

Figure 8: Uncorrelated errors

One important factor for the data quality is the presence of biases in the measurements. They lead to systematic errors in the positions computed and can also impact the time-to-fix. Figure 9 displays the biases derived for the data sets.
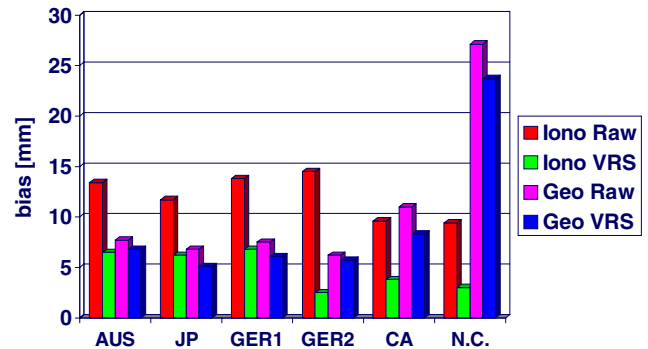

Figure 9:Biases

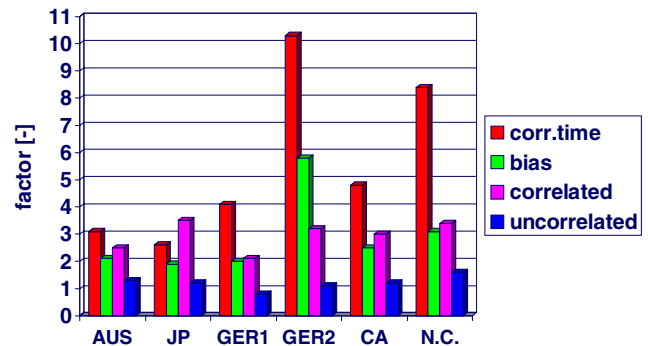The following figures summarize the improvement factors for all the information shown before.
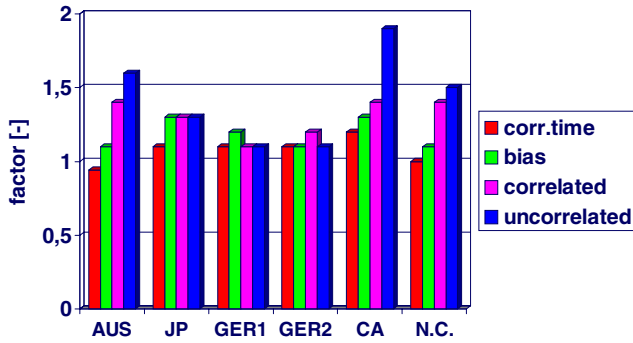

Figure 10: Ionosphere improvements

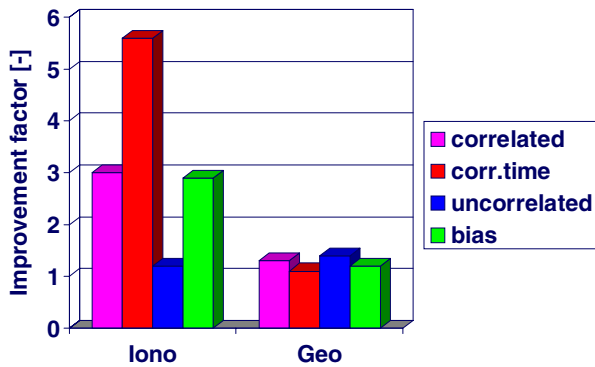**Figure 11: Geometric residual improvements**

Figure 12: Mean improvements

EFFECTS OF THE IMPROVEMENTS

The improvements achieved when using VRS were the initial motivation for this study. Nevertheless, an example follows to visualize one improvement the VRS user can expect.

In Figure 13 an example is given for the effect of the improvement of the geometric residuals on the positioning performance, i.e. the performance indicator the user is finally interested in.
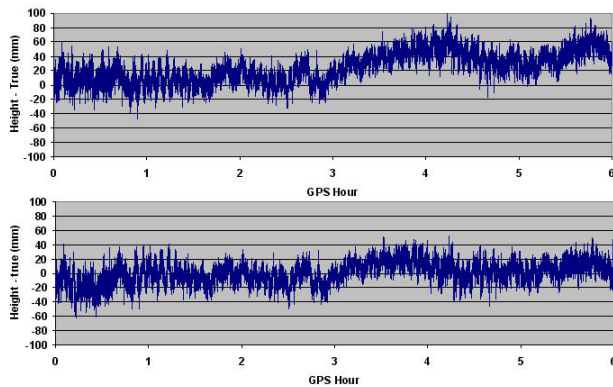

Figure 13: Height performance without and with VRS

While the raw data (upper graph) shows systematic effects up to 8 cm in the height component, this could be reduced to 4 cm by using VRS. Additional investigations proved that the origin of this height error is a strong tropospheric error in the data.

CONSEQUENCES

The VRS technique has proven the potential to reduce several main error sources in GPS positioning. For the ionosphere impact, most error characteristics have an average improvement factor between 2 and 10. It should be noted here that these improvements would be even higher if day data only would be analyzed, one proposal for continuing this study. Uncorrelated noise is reduced less, but still in a way that can be significant for kinematic applications.

Geometric errors, and, as the broadcast orbits are very good since a while, mainly tropospheric residuals are also reduced up to 40 % leading to improved positioning. Here a still a potential for further improvements to go to the limits of what can be achieved for a local effect like tropospheric errors.

The most surprising result was the presence of very high correlation times in both the ionospheric and the geometric errors in the range of 1 hour. The consequence is that simple averaging techniques are by far not sufficient for productive RTK positioning as here the user expects a time-to-fix in the tens of seconds to few minutes.

There are two coexisting solutions for this problem. The first is to implement more information about the errors into the RTK system algorithms, i.e. physical modeling of the ionosphere, tropospheric scaling techniques, etc. The other method is application of the VRS technique. As has been demonstrated, especially for the ionospheric errors the magnitude, but even more the correlation times of the errors are significantly reduced. This provides a new insight about how VRS-assisted RTK works.

Taking the changes in the error characteristics into account, RTK systems could benefit even more from the use of reference station networks. More research has been started to exploit the VRS potential to the maximum.

ACKNOWLEDGEMENTS

REFERENCES

[1] Wild, U., Beutler, G., Gurtner, W. and Rothacher, M: *Estimating the Ionosphere using One or More Dual Frequency GPS Receivers.* Proceedings of the 5th International Geodetic Symposium on Satellite

Positioning, Las Cruces, New Mexico, March 13-17, 1989.

[2] Sjöberg, L: The Best Linear Combination of L1 and L2 Frequency Observables in the Application of Transit/Doppler and GPS, manuscripta Geodetica 15 (1990), p. 17-11.

[3] Beutler, G., Schaer, S. and Rothacher, M.: *Wide Area Differential GPS, Study in the Context of AGNES*. Printing Office, University of Bern, September 17, 1999

[4] Talbot, N., Lu, G., Allison, T. and Vollath, U.: *Broadcast Network RTK – Transmission Standards and Results*, Accepted for Proceedings of the ION GPS 2002, Sep. 2002

[5] Trimble, 2002, *Trimble Virtual Reference Station (VRS)*, product brochure, Sunnyvale, California, 8 pages.(available at: http://www.trimble.com/vrs.html)

[6] Vollath, U., Buecherl, A., Landau, H. Pagels, C., Wagner, B.: *Multi-Base RTK using Virtual Reference Stations*, Proceedings of ION GPS 2000, Salt Lake City, Utah, September 19-22.

[7] Vollath, U., A. Buecherl, H. Landau, C. Pagels, B. Wagner, 2000a, Long-Range RTK Positioning Using Virtual Reference Stations, ION-GPS-2000, Salt Lake City, Utah.

[8] Vollath, U., A. Buecherl, H. Landau, C. Pagels, 2001, Long-Range RTK Positioning Using Virtual Reference Stations, KIS-2001.

[9] Aarons, J. and B. Santimay, 1994, Ionospheric Amplitude and Phase Fluctuations at the GPS Frequencies, Proceedings of ION-GPS-94, Salt Lake City, Utah, September 20-23.

[10] Colombo, O.L, et.al., 1999, Resolving Carrier-Phase Ambiguities On The Fly, At More Than 100km from Nearest Reference Site, with the help of Ionospheric Tomography, ION-GPS-99, Nashville, Tennessee, September.

[11] Essex, E. 1997, Ionospheric Effects on GPS Measurement, Proceedings of the Satellite Navigation Technology – 1997 & Beyond, Conference, Sydney, April 8-10.

[12] Goad, C.C. and L. Goodman, 1974, A modified Hopfield tropospheric correction model, Presented at the American Geophysical Union Fall Annual Meeting, San Francisco, December 12-17.

[13] Han, S. and C. Rizos, 1996, GPS Network Design and Error Mitigation for Real-Time Continuous Array Monitoring Systems, ION-GPS-96, Kansas City, Missouri, September 17-20. pp.1827-1836.

[14] Klobuchar, J.A., and P.H. Doherty, 1998, A Look Ahead: Expected Ionospheric Effects on GPS in 2000, GPS Solutions, Vol.2, No.1, pp.42-48.

[15] Raquet, J., 1998, Development of a Method for Kinematic GPS Carrier-Phase Ambiguity Resolution using Multiple Reference Stations, PhD Thesis, UCGE Report: 20116, The University of Calgary.

[16] Saastamoinen, J, 1972, Atmospheric correction for the troposphere and stratosphere in radio ranging of satellites, in The Use of Artificial Satellites for Geodesy, Geophys. Monogr. Ser.,vol 15,AGU, Washington, D.C. pp.247-251.

[17] Schaer, S. 1999, Mapping and Predicting the Earth's Ionosphere Using the Global Positioning System, PhD Thesis, Astronomic Institute, University of Bern.

Data Set		Ionospheric Residuals				Geometric Residuals			
		t_{cor} [sec]	bias [mm]	σ_{cor} [mm]	σ_{unc} [mm]	t_{cor} [sec]	bias [mm]	σ_{cor} [mm]	σ_{unc} [mm]
Australia	31 km	3290	13.4	57.4	6.6	1221	7.7	25.2	7.5
	VRS	1052	6.5	22.8	4.9	1304	6.8	17.7	4.6
	f_{impr}	3.1	2.1	2.5	1.3	0.94	1.1	1.4	1.6
Japan	26 km	1977	11.7	51.0	6.9	472	6.8	16.2	7.9
	VRS	771	6.2	14.7	5.8	448	5.1	12.9	6.1
	f_{impr}	2.6	1.9	3.5	1.2	1.1	1.3	1.3	1.3
Germany 1	19 km	2835	13.8	36.7	1.1	868	7.5	25.6	1.2
	VRS	693	6.8	17.3	1.4	815	6.1	23.9	1.1
	f_{impr}	4.1	2.0	2.1	0.8	1.1	1.2	1.1	1.1
Germany 2	31 km	4557	14.5	41.9	7.5	3103	6.2	21.4	8.0
	VRS	442	2.5	13.1	7.0	2818	5.7	17.5	7.3
	f_{impr}	10.3	5.8	3.2	1.1	1.1	1.1	1.2	1.1
California	25 km	3008	9.6	53.1	5.0	2958	11.0	21.6	5.6
	VRS	623	3.8	17.6	4.3	2426	8.3	15.9	3.0
	f_{impr}	4.8	2.5	3.0	1.2	1.2	1.3	1.4	1.9
N.Carolina	27 km	3772	9.4	36.2	6.2	4367	27.1	39.5	6.7
	VRS	450	3.0	10.6	3.8	4343	23.7	28.0	4.4
	f_{impr}	8.4	3.1	3.4	1.6	1.0	1.1	1.4	1.5
Mean	f_{impr}	5.6	2.9	3.0	1.2	1.1	1.2	1.3	1.4

Table 1: Overview of all test results